Optimizing detector thickness in dual-shot dual-energy x-ray imaging

Dong Woon Kim [a], Soohwa Kam [a], Hanbean Youn [a], Ho Kyung Kim [a,b*]
[a] School of Mechanical Engineering, Pusan National University, Busan, South Korea
[b] Center for Advanced Medical Engineering Research, Pusan National University, Busan, South Korea
[*] Corresponding author: hokyung@pusan.ac.kr

1. Introduction

The projection of three-dimensional (3D) human body on a two-dimensional (2D) radiograph results in the superimposition of normal tissue that can obscure abnormalities and in some common cases be misread as abnormalities. As a result, there exist apparent limitations in the conventional two-dimensional (2D) radiography: One is that the contrast between the structure of interest and the background in a radiograph is much less than the intrinsic subject contrast (i.e. the difference between their attenuation coefficients [1]; Another is that the superimposed anatomical structures in the 2D radiograph results in an anatomical background clutter that may decrease the conspicuity of subtle underlying features. These limitations in spatial and material discrimination are important motivations for the recent development of 3D (e.g. tomosynthesis) and dual-energy imaging (DEI) systems [2].

DEI technique uses a combination of two images obtained at two different energies in successive x-ray exposures by rapidly switching the kilovolage (kV) applied to the x-ray tube. Commercial DEI systems usually employ a "single" of flat-panel detector (FPD) to obtain two different kV images. However, we have a doubt in the use of the same detector for acquiring two different projections for the low- and high-kV setups because it is typically known that there exists an optimal detector thickness regarding specific imaging tasks or energies used [3].

To investigate the optimal detector thicknesses for the low- and high-kV images, we develop a theoretical model describing the energy-dependent detector signal and noise, and apply the developed model to the cost-benefit analysis on the use of dual detectors for DEI. Otherwise, we suggest the optimal thickness of the single detector for DEI.

2. Materials and Methods

2.1 Cascaded-systems analysis

We have developed a cascaded-systems model describing the signal and noise propagation through the image-forming processes in FPDs: α is the probability of x-ray interaction in the scintillator, β is the conversion gain to optical quanta, e is the scatter operation on the optical quanta with a probability density function $\mathrm{pr}(\underline{r})$, η is the selection probability of optical quanta in the photodiode, the integration implies the spatial summation of the selected quanta within an aperture, and σ_e is the RMS noise value due to readout noise. Then, we can respectively have the signal and noise as follows.

$$\bar{d}(E) = \bar{q}_0(E)ka^2\alpha(E)\beta(E)\eta(E) = \bar{q}_0(E)\bar{g}(E) \qquad (1)$$

and

$$\sigma_q^2(E) = \int_{-\infty}^{\infty}\int_{-\infty}^{\infty} \mathrm{NPS}_{pre}(u,v;E)\mathrm{d}u\mathrm{d}v$$
$$= \bar{q}_0(E)\bar{g}^2(E)\left[\frac{1}{a^2\alpha(E)\beta(E)\eta(E)}\right. \qquad (2)$$
$$\left. + \frac{1}{A_{eff}}\left(\frac{1}{\alpha(E)I(E)} - \frac{1}{\alpha(E)\beta(E)}\right)\right]$$

where $\bar{q}_0$ is incident x-ray spectrum, a is the pixel aperture, and I is the Swank noise factor. The effective aperture A_{eff} is given by

$$A_{eff} = \left[\int_{-\infty}^{\infty}\int_{-\infty}^{\infty} T_{tot}^2(u,v)\mathrm{d}u\mathrm{d}v\right]^{-1}$$
$$= \left[\int_{0}^{f_{Ny}} 2\pi f T_{tot}^2(f)\mathrm{d}f\right]^{-1} \qquad (3)$$

where $T_{tot}(f) = T_X(f)\times T_O(f)\times T_P(f)$, and T_X, T_O, and T_P denote the x-ray, optical, and pixel modulation transfer functions (MTFs), respectively.

Therefore, detective quantum efficiency (DQE) is represented by

$$\mathrm{DQE}(E) = \frac{\bar{d}^2(E)}{\bar{q}_o(E)\left[A_{eff}\sigma_q^2(E) + p^2\sigma_e^2\right]} \qquad (4)$$

where p is pixel pitch.

For the quantitative evaluation of optimal detector thickness combination, we calculate a figure of merit (FOM) of the enhanced material j against the background in dual-energy images:

$$FOM_j = \frac{CNR_j^2}{X} = \frac{C_j^2}{X\sigma_j^2}$$
$$= (\Delta\bar{\mu}_{jM}^H - w_j\Delta\bar{\mu}_{jM}^L)^2 t_j^2 \qquad (5)$$
$$\times\left[\frac{1}{\bar{q}_0^H A_X^H DQE^H A_{eff}^H}\right.$$
$$\left. + \frac{w_j^2}{\bar{q}_0^H(1-A_X^H)DQE^H A_{eff}^H}\right]^{-1}$$

where C_j is contrast of the enhanced material j against the background, X is total exposure used for low- and high-kV projections, and A_X^H is allocation of high- kV. The FOM consists of squared contrast-to-noise ratio (CNR) and the normalized exposure X.
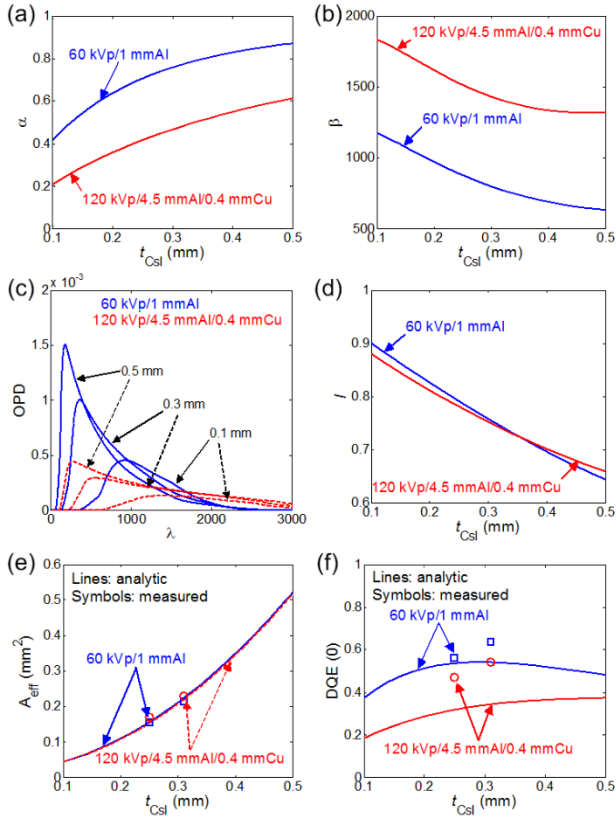
Fig. 1. Calculation results of the cascaded-systems model parameters. (a) Quantum collection efficiency (b) quantum conversion gain (c) optical-pulse height distribution (d) swank noise factor (e) effective aperture (f) detective quantum efficiency.

2.2 Validation

To validate the theoretical model, we compared the calculation results with experimental results. To measure the A_{eff} and the DQE(0), we measured MTF and noise-power spectrum (NPS). We used the 60 kV/1 mmAl and 120 kV/4.5 mmAl/0.4 mmCu for the low and high kV energies, respectively [4]. We used a FPD that consisted of a CsI scintillator (250 μm or 310 μm) optically coupled to a CMOS photodiode array (RadEye1™, Teledyne Rad-icon Imaging Corp., Sunnyvale, CA).

3. Preliminary results

Fig. 1 summarizes the model parameters used for the CSA. Fig. 1(a) shows that the quantum efficiency increases with increasing scintillator CsI thickness. Fig.1 (b) shows the production of secondary quanta (i.e. optical quanta) at the exit side of the CsI layer considering the secondary-quantum loss mechanism during their transports within the CsI layer. Swank factors, as shown in fig. 1(d), are calculated using the optical pulse-height distributions as demonstrated in fig. 1(c). Figs. 1(e) and (f) show the calculated A_{eff} and DQE, respectively, including the measured data. The calculated A_{eff} agrees well with the measured data. Some discrepancies between the calculated and measured DQE are observed. Further investigation is needed.

Fig. 2 is the 2D contour plots of FOM and contrast that are normalized by the maximum values. The x-axis is the
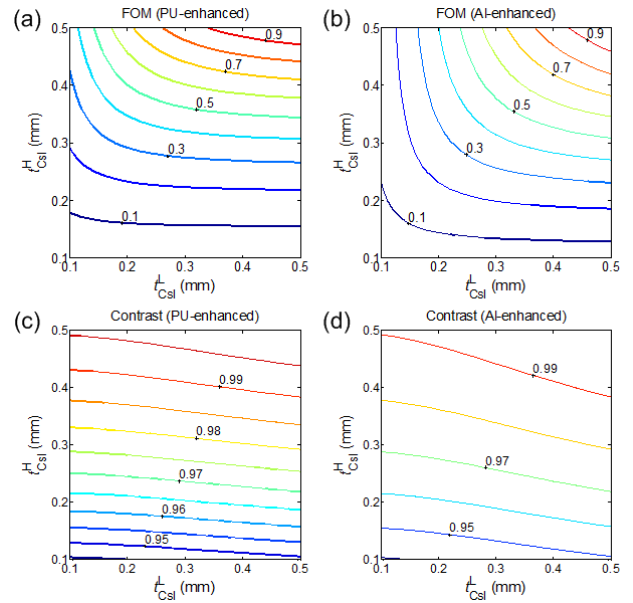

Fig. 2. Exposure-normalized squared-CNR values and contrast for the detector thickness combination in low- and high-energy setup (the following 2D contour plots are normalized by the maximum values). (a) PU-enhanced FOM (b) Al-enhanced FOM (c) PU-enhanced contrast (d) Al-enhanced contrast.
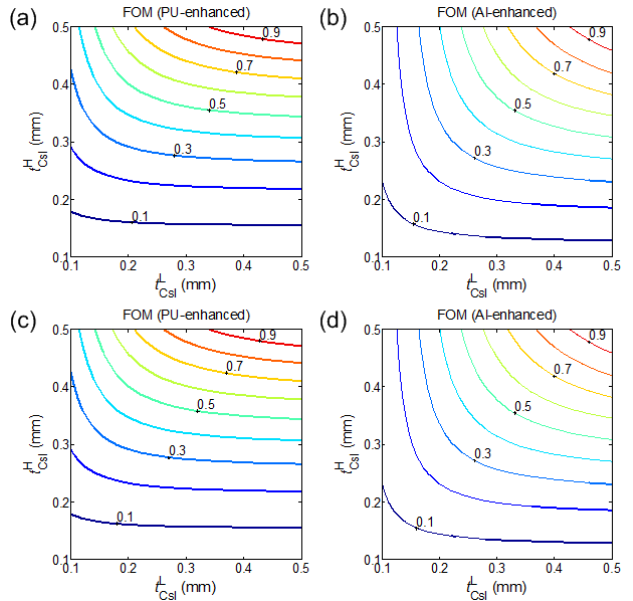

Fig. 3. Effect of electronic noise on exposure-normalized squared-CNR values. (a) PU-enhanced FOM ($\sigma_e = \sigma_q$) (b) Al-enhanced FOM ($\sigma_e = \sigma_q$) (c) PU-enhanced FOM ($\sigma_e = 5 \times \sigma_q$) (d) Al-enhanced FOM ($\sigma_e = 5 \times \sigma_q$).

scintillator thickness for the low kV and y-axis is the scintillator thickness for the high kV imaging, respectively. Figs. 2(a) and (b) show the PU-enhanced and Al-enhanced FOM, respectively. In the case of the Al-enhanced FOM, the influence of the scintillator thickness for the low and high kV are similar. But for the PU-enhanced FOM, the influence of the scintillator thickness for high kV is 20 times greater than that of the scintillator thickness for the low kV. Figs. 2(c) and (d) show the PU-enhanced and Al-enhanced contrast, respectively. The contrast is sensitive to the CsI scintillator thickness for high kV. Since all the

simulations were performed at the same total exposure, the differences between the FOM and contrast results can be explained by noise.

Fig. 3 shows the changes in the FOM due to the increased electronic noise. Figs. 3(a) and (b) show that additive electronic noise level is the same as the quantum noise level. Figs. 4(c) and (d) show that additive electronic noise level is 5 times larger than the quantum noise level. The influence of σ_e on the FOM can be negligible.

3. Conclusions

In this study, by using DEI techniques, we expected to be exist the scintillator thickness combination indicating the optimal FOM performance. We calculated FOM by using the CSA model applied optical photon escape probability. Signal and noise in dual-energy imaging has been modeled and validated with the measurements (DQE(0) and A_{eff}). The best FOMs for PU- and Al-enhanced dual-energy images are obtained when the thickest CsI (i.e. ~0.5 mm in this study) are used in both high- and low-kV imaging. To obtain a higher FOM_{PU} (i.e. soft tissue), use of a thicker CsI scintillator thickness with high energy is more critical than CsI scintillator thickness with low energy. The FOM_j performance is almost independent of the level of detector electronic noise, but is mainly dependent on the quantum noise. We conclude that a single detector can be used for the double-shot DEI.

ACKNOWLEDGEMENT

REFERENCES

[1] L. A. Lehmann, R. E. Alvarez, A. Macovski, and W. R. Brody, Generalized image combinations in kVp digital radiography, Med. Phys., Vol.8, pp.659-667, 1981.
[2] N. A. Shkumat, J. H. Siewerdsen, A. C. Dhanantwari, D. B. Williams, S. Richard, S. Paul, J. Yorkston, and R. V. Metter, Optimization of image acquisition techniques for dual-energy imaging of the chest, Med. Phys., Vol.34, pp.3904-3915, 2007.
[3] J. H. Siewerdsen, and L. E. Antonuk, DQE and system optimization for indirect-detection flat-panel imagers in diagnostic radiography, Proc. SPIE, Vol.3336, pp.546–556, 1998.
[4] J. H. Siewerdsen, N. A. Shkumat, A. C. Dhanantwari, D. B. Williams, S. Richard, M. J. Daly, N. S. Paul, D. J. Moseley, D. A. Jaffray, J. Yorkston, and R. Van Metter, High-performance dual-energy imaging with a flat-panel detector: imaging physics from blackboard to benchtop to bedside, Proc. SPIE, Vol. 6142, pp. 61421E, 2006